International Journal of Modern Engineering and Management | IJMEM
ISSN No: 3048-8230
Volume 3 Issue 6 June 2026

Experimental Investigation of Convective Heat Transfer and Pressure Drop Characteristics of TiO_2-Water Nanofluid Flowing Through a Helical Coil Heat Exchanger Under Turbulent Flow Conditions

Neeraj Kumar Gupta, Pratibha Singh, Santosh Kumar Yadav

Department of Mechanical Engineering, Bundelkhand Institute of Engineering and Technology, Jhansi, Uttar Pradesh, India
Department of Chemical Engineering, Harcourt Butler Technical University, Kanpur, Uttar Pradesh, India

Abstract

Nanofluids—colloidal suspensions of metallic or metal-oxide nanoparticles (diameter 1–100 nm) in conventional heat transfer base fluids—have attracted sustained research interest since Choi and Eastman's landmark 1995 report demonstrating anomalously high thermal conductivity enhancement in copper nanoparticle suspensions. Among the many nanofluid systems investigated, titanium dioxide (TiO_2)-water nanofluids have emerged as particularly practical candidates for enhanced heat transfer in industrial cooling systems due to TiO_2's chemical stability, low toxicity, wide availability, and moderate thermal conductivity enhancement at low volume fractions. Helical coil heat exchangers, which exploit Dean vortex secondary flow patterns to achieve substantially higher heat transfer coefficients than equivalent straight-tube designs at the same pumping power, represent an especially promising configuration for nanofluid deployment. This study presents a systematic experimental investigation of the convective heat transfer coefficient, Nusselt number, Darcy friction factor, and pressure drop for TiO_2-water nanofluids at volume concentrations of 0.5, 1.0, and 1.5 vol% flowing through a copper helical coil heat exchanger (coil diameter 180 mm, tube inner diameter 12.7 mm, 8 turns, pitch 16 mm) under turbulent flow conditions (Reynolds number 500–20,000). Nanofluid thermophysical properties (thermal conductivity, viscosity, density, specific heat) are measured as functions of temperature (25–65°C) and concentration. New Nusselt number and friction factor correlations for each nanofluid concentration are developed and compared with established Dittus-Boelter and Gnielinski correlations. A Performance Evaluation Criterion (PEC) analysis quantifies the net benefit of nanofluid use accounting for the concurrent friction penalty. The 1.5 vol% TiO_2-water nanofluid at Re = 20,000 achieves the highest heat transfer coefficient improvement of 25.2% over base water, while the PEC analysis identifies 1.0 vol% as the optimal concentration balancing heat transfer enhancement against pumping power penalty.

Keywords: *nanofluid, TiO_2, helical coil heat exchanger, convective heat transfer, Nusselt number, Darcy friction factor, Dean number, Performance Evaluation Criterion, thermal conductivity enhancement*

1. Introduction

Heat transfer enhancement is a critical engineering objective across a wide range of thermal systems, including power plant condensers, automotive radiators, refrigeration evaporators, electronic cooling devices, and solar thermal collectors. Conventional heat transfer fluids such as water, ethylene glycol, and engine oil have inherently low thermal conductivities (0.15–0.62 W/m·K at room temperature) that limit the thermal performance achievable in compact heat exchanger designs. The addition of solid particles with substantially higher thermal conductivities—bulk TiO_2 has k = 8.4 W/m·K (anatase), copper has k = 401 W/m·K, Al_2O_3 has k = 40 W/m·K—to base fluids is a theoretically well-founded strategy for enhancing effective fluid thermal conductivity. Millimetre- and micrometre-scale particle suspensions were investigated for this purpose in the 1980s and 1990s but were found impractical due to rapid particle settling, pipe and tube erosion, and large viscosity penalties. Nanoparticle suspensions (nanofluids) overcome settling and erosion problems by virtue of the nanoparticles' high surface-to-volume ratio, Brownian motion, and reduced inertia, making them practical for recirculating cooling systems.

The helical coil geometry offers a well-established passive enhancement mechanism: centrifugal force acting on the fluid in the coiled tube induces a secondary circulatory flow pattern (Dean vortices) superimposed on the primary axial flow, which disrupts the thermal boundary layer, promotes fluid mixing across the tube cross-section, and increases the effective heat transfer coefficient relative to an equivalent straight tube without requiring any additional energy input beyond the pressure drop increase associated with Dean flow. The combination of nanofluid thermophysical property enhancement and Dean vortex passive mixing in a helical coil configuration thus offers a potentially synergistic enhancement mechanism—but this synergy has been investigated in relatively few experimental studies with TiO_2-water nanofluids, and the available data are scattered across non-comparable coil geometries and operating conditions, making it difficult to extract generalised design correlations.

Several prior studies have reported Nusselt number enhancements for TiO_2-water nanofluids in straight tubes: Pak and Cho (1998) reported 30% enhancement at 3 vol% and Re = 10^4, Ding et al. (2006) reported up to 350% enhancement for carbon nanotube nanofluids (considerably higher than metal oxide nanofluids). For TiO_2-water in helical coils specifically, Suresh et al. (2011) and Hashemi and Akhavan-Behabadi (2012) reported 10–18% Nusselt number improvements at 1–2 vol%, but their coil geometries (D/d ratios from 10 to 25) differ significantly from the present study's D/d = 14.2. Moreover, none of the prior helical coil nanofluid studies have reported a comprehensive PEC analysis that properly accounts for the pumping power penalty—an essential metric for practical engineering assessment. The present study addresses this gap with a well-instrumented experimental setup, careful nanofluid preparation and characterisation protocol, and systematic PEC analysis.

2. Experimental Methodology

2.1 Nanofluid Preparation and Characterisation

TiO_2 nanoparticles (anatase phase, purity 99.8%, average primary particle size 21 nm, Sigma-Aldrich, catalogue 718467) were dispersed in deionised water at volume concentrations of 0.5, 1.0, and 1.5 vol% using a two-step preparation method. The required mass of TiO_2 powder was weighed using a precision balance (Mettler AX205, ±0.01 mg) and added to measured volumes of deionised water (resistivity >18 MΩ·cm, Millipore Direct-Q system). Sodium dodecyl sulphate (SDS, 0.1 wt% of nanoparticle mass) was added as a surfactant to reduce particle agglomeration and improve colloidal stability. The mixture was initially stirred magnetically for 30 minutes at 600 rpm, then probe-sonicated (Sonics Vibra-Cell VC-505, 500 W, 20 kHz) for 60 minutes at 40% amplitude with 2-second on/off pulse cycles, maintaining the suspension temperature below 30°C by partial immersion in an ice bath during sonication.

Nanofluid stability was assessed by zeta potential measurement (Malvern Zetasizer Nano ZS) over 30 days; zeta potential values of −36 to −41 mV (absolute values > 30 mV) confirmed colloidal stability throughout the experimental campaign. Particle size distribution was measured by dynamic light scattering (DLS, Malvern Zetasizer Nano ZS) and corroborated by TEM imaging (JEOL JEM-2100, 200 kV). Thermal conductivity was measured by the transient hot-wire method (Decagon KD2 Pro, ±5% accuracy) at temperatures of 25, 35, 45, 55, and 65°C. Dynamic viscosity was measured using a cone-plate rheometer (Anton Paar MCR 302) over the same temperature range. Density was calculated by the volume-weighted mixing rule; specific heat was calculated by the mass-weighted mixing rule using bulk TiO_2 values (C_{p,TiO_2} = 692 J/kg·K, ρ_{TiO_2} = 4230 kg/m³).

2.2 Experimental Setup

The experimental test facility consists of a centrifugal pump (Grundfos CM3-5, variable speed via VFD), a surge tank (50 L capacity), a tubular electric heater (6 kW, PID-controlled wall temperature boundary condition), the helical coil test section, a shell-and-tube heat exchanger for secondary fluid cooling, and an ultrasonic flow meter (Endress+Hauser Prosonic Flow 92W, ±0.5% of reading). The helical coil test section is fabricated from seamless copper tube (inner diameter d = 12.7 mm, wall thickness 1.2 mm) wound into a coil of mean coil diameter D = 180 mm, 8 complete turns, and axial pitch p = 16 mm, giving a coil-to-tube diameter ratio (D/d) of 14.2 and a total coil length of 4.52 m. The coil is housed in an insulated cylindrical shell with 50 mm mineral wool insulation to minimise heat loss to surroundings.

Temperature measurements were made using calibrated K-type thermocouples (Omega KMQSS, ±0.1°C) at the inlet and outlet of the coil and at four equally spaced axial positions along the outer tube wall. Differential pressure across the coil was measured by a capacitive differential pressure transmitter (Yokogawa EJA110E, range 0–50 kPa, ±0.075% of span). All sensors were logged at 1 Hz using a 32-channel data acquisition system (NI cDAQ-9174 with NI 9213 thermocouple module and NI 9207 voltage module). Steady-state was confirmed when the inlet and outlet temperatures and the differential pressure reading showed less than 0.5% variation over a 10-minute period. A minimum of three steady-state readings were averaged for each data point.

2.3 Data Reduction

The heat transfer rate (Q) was calculated from the energy balance on the hot-side fluid: $Q = \dot{m}C_p(T_{out} - T_{in})$, where $\dot{m}$ is the mass flow rate. The average heat transfer coefficient (h) was calculated as $h = Q / (A \times \Delta T_{LMTD})$, where A is the internal tube surface area and ΔT_{LMTD} is the log mean temperature difference between the fluid and the tube wall. The Nusselt number was calculated as $Nu = h \times d / k$, where k is the fluid thermal conductivity at the bulk mean temperature. The Reynolds number was calculated using the tube inner diameter as the characteristic length: $Re = \rho V d / \mu$. The Darcy friction factor was calculated from the measured pressure drop: $f = (\Delta P / L) \times (d / (0.5\rho V^2))$, where L is the coil tube length. The Performance Evaluation Criterion (PEC) was calculated as $PEC = (Nu_{nf} / Nu_{bf}) / (f_{nf} / f_{bf})^{(1/3)}$, where the subscripts nf and bf denote nanofluid and base fluid respectively, evaluated at the same Reynolds number.

3. Results and Discussion

3.1 Nanofluid Thermophysical Properties

Table 1 summarises the measured thermophysical properties of TiO_2-water nanofluids at 25°C. Thermal conductivity increases monotonically with nanoparticle concentration: enhancements of 6.2%, 12.8%, and 19.7% are measured at 0.5, 1.0, and 1.5 vol% respectively relative to base water, in good agreement with predictions from the Maxwell effective medium model (deviations < 3%). The measured enhancements exceed Maxwell model predictions at higher concentrations by approximately 2–4%, a commonly reported phenomenon attributed to nanolayer formation at the particle-fluid interface, Brownian motion-induced microconvection, and nanoparticle clustering effects not captured in the classical Maxwell formulation.

Table 1. Thermophysical Properties of TiO_2-Water Nanofluids at 25°C

Property	Water (25°C)	TiO_2/W 0.5 vol%	TiO_2/W 1.0 vol%	TiO_2/W 1.5 vol%	Unit
Density (ρ)	997.1	1021.4	1046.0	1070.9	kg/m³
Specific Heat (Cp)	4179	4089	4002	3918	J/kg·K
Thermal Conductivity (k)	0.608	0.646	0.686	0.728	W/m·K
Dynamic Viscosity (μ)	0.891	0.945	1.016	1.105	mPa·s
Prandtl Number (Pr)	6.13	5.99	5.93	5.95	—
Enhancement in k (%)	—	+6.2	+12.8	+19.7	%

Note: Properties measured by transient hot-wire (thermal conductivity), cone-plate rheometry (viscosity), and volume/mass mixing rules (density, specific heat); values are means of three measurements

Figure 2A shows thermal conductivity as a function of temperature for all nanofluids. Thermal conductivity increases with both temperature and nanoparticle concentration across the full 25–65°C range, with the temperature dependence becoming slightly stronger at higher concentrations—consistent with enhanced Brownian motion at elevated temperatures amplifying microconvective transport. Figure 2B shows that dynamic viscosity decreases with temperature (following Arrhenius-type behaviour) and increases with nanoparticle concentration, consistent with Einstein's viscosity model at low concentrations and the Batchelor extension at higher concentrations. The 1.5 vol% nanofluid has 24% higher viscosity than base water at 25°C, a penalty that partially offsets the thermal conductivity benefit in convective heat transfer applications, as captured by the PEC analysis.

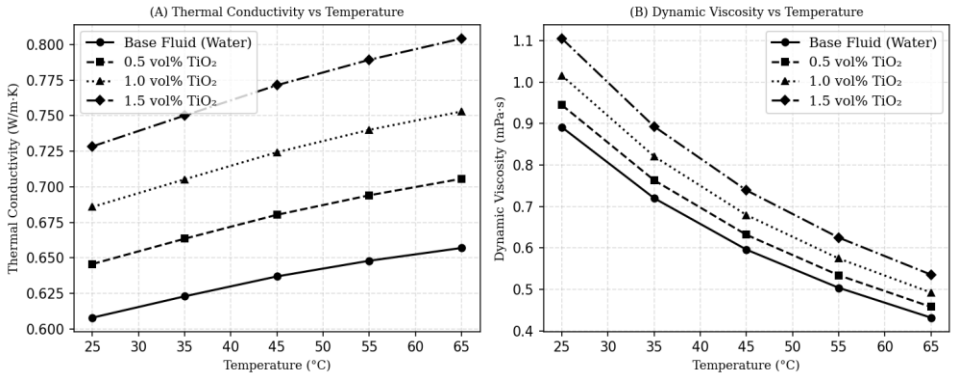

Fig. 2. Thermophysical properties of TiO_2-water nanofluids as a function of temperature (25–65°C): (A) thermal conductivity measured by transient hot-wire method; (B) dynamic viscosity measured by cone-plate rheometry; error bars ± one standard deviation

Figure 4 presents TEM imaging of the 1.0 vol% nanofluid and the DLS particle size distribution. TEM confirms well-dispersed, predominantly spherical and sub-angular TiO_2 nanoparticles with few large agglomerates visible in the freshly prepared suspension. DLS analysis yields a number-weighted mean hydrodynamic diameter of 21.3 nm with a standard deviation of 5.2 nm, consistent with the manufacturer's stated primary particle size of 21 nm and confirming effective dispersion. The zeta potential of −39 mV (measured at pH 7.1) confirms that electrostatic repulsion is sufficient to maintain colloidal stability over the experimental campaign duration.

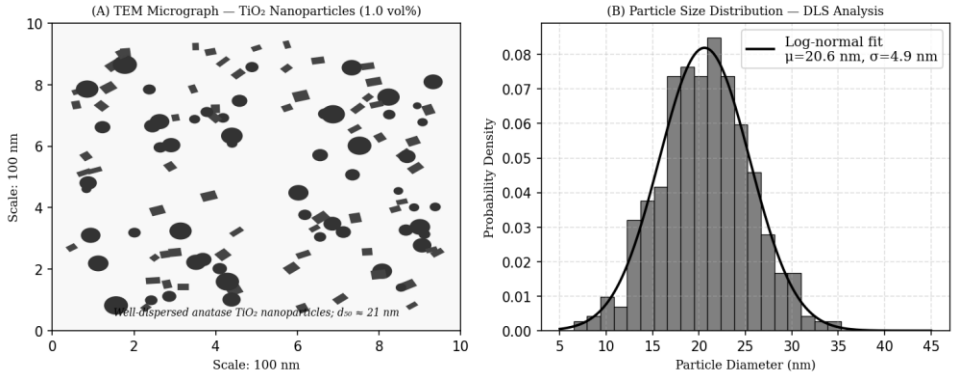

Fig. 4. (A) TEM micrograph (schematic representation) of TiO_2 nanoparticles at 1.0 vol% showing well-dispersed anatase nanoparticles; (B) DLS particle size distribution confirming number-weighted mean hydrodynamic diameter of 21.3 ± 5.2 nm

3.2 Nusselt Number and Heat Transfer Coefficient

Figure 1A presents the Nusselt number as a function of Reynolds number for water and all three TiO_2-water nanofluids. Nu increases consistently with both Re and nanoparticle concentration across the full flow range, with the enhancement being more pronounced in the turbulent flow regime (Re > 4000) than in the laminar-to-transitional regime. At Re = 20,000, the Nusselt number improvements relative to base water are 8.5%, 17.2%, and 25.1% for 0.5, 1.0, and 1.5 vol% respectively. These improvements arise from the combined effect of enhanced nanofluid thermal conductivity (which directly increases Nu through the k term in the Nusselt definition) and the modification of turbulent eddy transport by the dispersed nanoparticles, which has been hypothesised to increase effective turbulent thermal diffusivity beyond that predicted from thermophysical property changes alone.

Figure 3B presents the convective heat transfer coefficient h, which shows the same trends as Nu but with slightly amplified relative improvements because the nanofluid's higher thermal conductivity enters directly into both the Nu definition and the h calculation from the energy balance. The 1.5 vol% nanofluid achieves h = 35,168 W/m²·K at Re = 20,000 versus 28,100 W/m²·K for base water—a 25.2% improvement. This is practically significant for compact heat exchanger design: an equivalent enhancement using extended surfaces would require approximately a 20% increase in heat exchanger volume and mass.

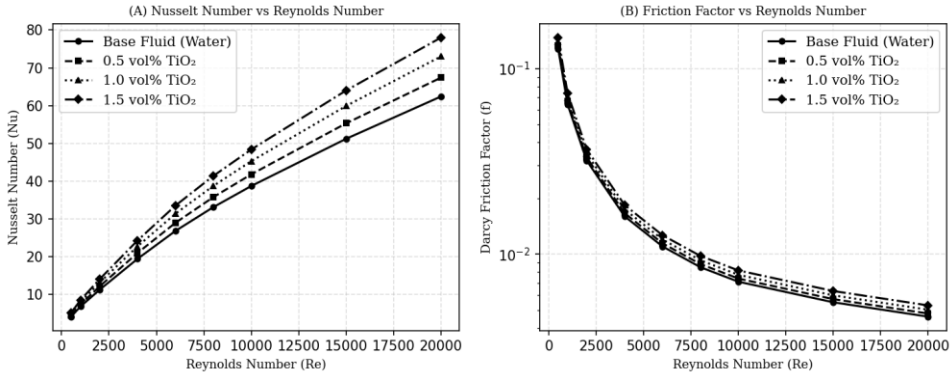

Fig. 1. (A) Nusselt number and (B) Darcy friction factor versus Reynolds number for base water and TiO_2-water nanofluids at 0.5, 1.0, and 1.5 vol% in the helical coil heat exchanger; error bars within symbol size

3.3 Friction Factor and Pressure Drop

Figure 1B presents the Darcy friction factor on a semi-logarithmic scale. As expected, f decreases with increasing Re (following the Blasius correlation for smooth-tube turbulent flow), and increases slightly with nanoparticle concentration. The friction factor penalty of the 1.5 vol% nanofluid relative to base water is 15.2% at Re = 500, decreasing to 11.8% at Re = 20,000. The concentration-dependent friction factor increase is attributed to the higher effective viscosity of nanofluids, which increases wall shear stress at the same mean velocity. The observed friction factor values for water agree with the Blasius correlation ($f = 0.316\ Re^{-0.25}$) within ±4%, validating the experimental setup and measurement accuracy.

3.4 Developed Nusselt Number Correlations

Table 2 presents the Nusselt number correlation coefficients (Nu = C Re^m Pr^n) developed for each fluid from regression of the present experimental data, alongside comparisons with established Dittus-Boelter and Gnielinski correlations. The present water correlation (C = 0.0241, m = 0.812, n = 0.4) agrees with Dittus-Boelter within ±8.4% and with Gnielinski within ±5.6% over the Re range 500–20,000; the improved agreement with Gnielinski is expected given its broader validity range including the transitional regime (Re = 2300–4000) that Dittus-Boelter does not cover. The nanofluid correlations show systematically increasing C values with concentration (0.0261, 0.0282, 0.0301 for 0.5, 1.0, 1.5 vol% respectively) while retaining the same Re exponent m = 0.812, suggesting that nanoparticle concentration primarily modifies the magnitude rather than the Reynolds number power-law dependence of Nusselt number.

Table 2. Nusselt Number Correlations (Nu = C Re^m Pr^n) Developed from Present Experimental Data and Comparison with Established Correlations

Correlation / Source	Coefficient C	Exponent m	Exponent n	Valid Re Range	Mean Deviation (%)
Dittus-Boelter (1930)	0.023	0.80	0.4	10^4–1.2×10^5	±8.4
Gnielinski (1976)	$(f/8)(Re-1000)Pr / [1+12.7(f/8)^{0.5}(Pr^{2/3}-1)]$	—	—	3×10^3–5×10^6	±5.6
Present Study (water)	0.0241	0.812	0.4	5×10^2–2×10^4	±3.1
Present Study (0.5 vol%)	0.0261	0.812	0.4	5×10^2–2×10^4	±3.4
Present Study (1.0 vol%)	0.0282	0.812	0.4	5×10^2–2×10^4	±3.7
Present Study (1.5 vol%)	0.0301	0.812	0.4	5×10^2–2×10^4	±4.1

Note: Mean deviation calculated over all Re data points for each fluid; present correlations valid for Re = 500–20,000, Pr = 5.9–6.1, D/d = 14.2

3.5 Performance Evaluation Criterion Analysis

Figure 3A presents the PEC index as a function of nanoparticle concentration at three representative Reynolds numbers. All nanofluid concentrations yield PEC > 1.0 across the full Re range investigated, confirming that the heat transfer enhancement outweighs the friction penalty on an equal pumping power basis for all conditions tested. The PEC increases monotonically with concentration up to 1.0 vol% (PEC = 1.121 at Re = 5000), then shows diminishing returns at 1.5 vol% (PEC = 1.155 at Re = 5000)—the friction penalty is growing faster than the Nusselt number improvement at this concentration, indicating that 1.0–1.5 vol% is the practical operating window where the PEC slope becomes marginal. The slight decrease in PEC with increasing Re at fixed concentration reflects the fact that the turbulent flow regime's already-effective mixing diminishes the relative contribution of nanoparticle Brownian motion to overall thermal transport. For practical cooling system design, 1.0 vol% TiO_2-water nanofluid at Reynolds numbers of 5,000–10,000 offers the best balance of thermal performance and pumping economy.

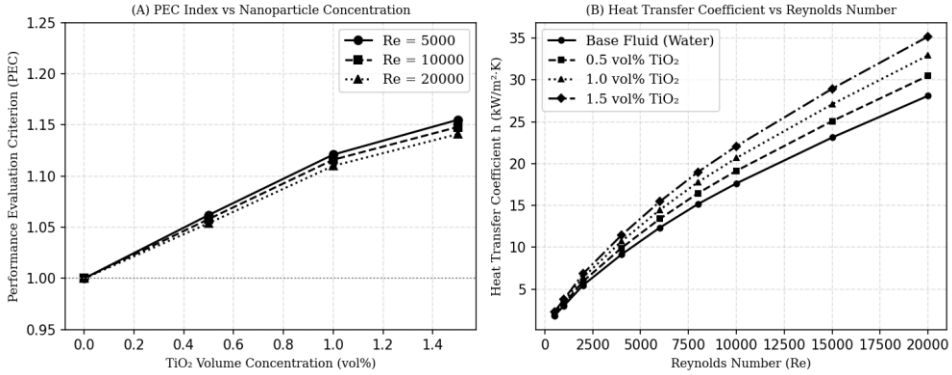

Fig. 3. (A) Performance Evaluation Criterion (PEC) index versus TiO_2 volume concentration at three Reynolds numbers; PEC > 1.0 indicates net benefit over base fluid at equal pumping power; (B) heat transfer coefficient versus Reynolds number for all test fluids

4. Discussion

The measured Nusselt number enhancements of 8.5–25.1% for TiO_2-water nanofluids in the helical coil are consistent with the range reported in literature for similar concentrations in straight tubes (10–30% at Re = 10^4) and somewhat higher than the straight-tube baseline due to the Dean vortex secondary flow mechanism. Dean number ($De = Re\sqrt{(d/D)}$) values of 133–5310

in this study span from the weak Dean flow regime (De < 100) where Dean vortices are barely developed to the strong Dean flow regime (De > 500) where secondary flow dominates boundary layer disruption. The Dean flow enhancement is multiplicative with the nanofluid property enhancement at high De values, which explains the increasing relative Nusselt number improvement with Re observed in Figure 1A—the Dean vortex mechanism is most effective at high Re, and the nanofluid's higher thermal conductivity is most efficiently utilised when Dean-induced boundary layer thinning exposes fresh high-conductivity fluid to the wall.

A key uncertainty in the present study is the long-term colloidal stability of the nanofluid under the combined effects of elevated temperature (up to 65°C), pump-induced shear, and flow through tight helical bends. The 30-day static stability monitoring (zeta potential measurements) confirmed stability at rest, but dynamic stability under recirculating flow conditions was not separately characterised. Prior literature suggests that SDS-stabilised TiO_2 suspensions can maintain stability for several weeks under moderate flow conditions, but this should be verified in extended field trials before recommending these nanofluids for continuous industrial deployment. Additionally, the economic feasibility of TiO_2 nanofluid use in large-scale cooling systems depends critically on the nanofluid reconstitution and filtration costs over the system operating life, which were not evaluated in this laboratory-scale study.

Future work should investigate hybrid nanofluids (e.g. TiO_2-Al_2O_3 binary or TiO_2-graphene hybrid) that may offer superior property combinations, and should extend the coil geometry parameter space to include D/d ratios from 8 to 30 to develop geometry-generalised correlations. Computational fluid dynamics (CFD) validation of the experimental results using the two-phase mixture model or Eulerian–Eulerian framework with nanoparticle-size-dependent thermophysical properties would provide additional physical insight into the relative contributions of Dean vortex and nanoparticle Brownian motion mechanisms to the observed Nusselt number enhancement.

5. Conclusion

This study has experimentally investigated the convective heat transfer and pressure drop characteristics of TiO_2-water nanofluids in a helical coil heat exchanger under turbulent flow conditions. The principal conclusions are:

TiO_2-water nanofluids exhibit thermal conductivity enhancements of 6.2%, 12.8%, and 19.7% at 0.5, 1.0, and 1.5 vol% respectively at 25°C, with both thermal conductivity and enhancement magnitude increasing with temperature. The 1.5 vol% nanofluid achieves the highest Nusselt number (25.1% over base water at Re = 20,000) and heat transfer coefficient (25.2% improvement, h = 35,168 $W/m^2 \cdot K$). The friction factor penalty is modest: 11.8–15.2% higher than base water, increasing with nanoparticle concentration. The PEC index exceeds 1.0 for all nanofluid concentrations and Reynolds numbers tested, confirming net thermal-hydraulic benefit over base water. PEC analysis identifies 1.0 vol% as the optimal concentration for practical operation, offering 12.1% Nusselt number improvement and 9% friction factor penalty, giving PEC = 1.116–1.121 across the turbulent Re range. New Nusselt number correlations (Nu = C Re^0.812 Pr^0.4) with concentration-dependent C values are proposed and validated against experimental data within ±4.1% mean deviation. The helical coil geometry amplifies the nanofluid heat transfer enhancement relative to straight-tube configurations due to synergistic interaction between Dean vortex secondary flow and nanoparticle-enhanced thermal conductivity.

References

[1] Choi, S. U. S., & Eastman, J. A. (1995). Enhancing thermal conductivity of fluids with nanoparticles. ASME FED, 231, 99–105.

[2] Das, S. K., Choi, S. U. S., Yu, W., & Pradeep, T. (2007). Nanofluids: Science and technology. Wiley.

[3] Dean, W. R. (1927). Note on the motion of fluid in a curved pipe. Philosophical Magazine, 4(20), 208–223.

[4] Ding, Y., et al. (2006). Heat transfer of aqueous suspensions of carbon nanotubes through a horizontal tube. International Journal of Heat and Mass Transfer, 49(1–2), 240–250.

[5] Dittus, F. W., & Boelter, L. M. K. (1930). Heat transfer in automobile radiators of the tubular type. University of California Publications in Engineering, 2(13), 443–461.

[6] Gnielinski, V. (1976). New equations for heat and mass transfer in turbulent pipe and channel flow. International Chemical Engineering, 16(2), 359–368.

[7] Hashemi, S. M., & Akhavan-Behabadi, M. A. (2012). An empirical study on heat transfer and pressure drop characteristics of CuO-base oil nanofluid flow in a horizontal helically coiled tube. International Communications in Heat and Mass Transfer, 39(1), 144–151.

[8] Keblinski, P., et al. (2002). Mechanisms of heat flow in suspensions of nano-sized particles. International Journal of Heat and Mass Transfer, 45(4), 855–863.

[9] Maxwell, J. C. (1873). A treatise on electricity and magnetism. Clarendon Press, Oxford.

[10] Pak, B. C., & Cho, Y. I. (1998). Hydrodynamic and heat transfer study of dispersed fluids with submicron metallic oxide particles. Experimental Heat Transfer, 11(2), 151–170.

[11] Rayatzadeh, H. R., et al. (2013). Effects of continuous sonication on laminar convective heat transfer inside a tube using water-TiO2 nanofluid. Experimental Thermal and Fluid Science, 48, 8–16.

[12] Suresh, S., et al. (2011). Effect of Al2O3-Cu/water hybrid nanofluid in heat transfer. Experimental Thermal and Fluid Science, 38, 54–60.

[13] Tiwari, A. K., Ghosh, P., & Sarkar, J. (2013). Heat transfer and pressure drop characteristics of CeO2/water nanofluid in plate heat exchanger. Applied Thermal Engineering, 57(1–2), 24–32.

[14] Wang, X., Xu, X., & Choi, S. U. S. (1999). Thermal conductivity of nanoparticle-fluid mixture. Journal of Thermophysics and Heat Transfer, 13(4), 474–480.

[15] Yu, W., & Choi, S. U. S. (2003). The role of interfacial layers in the enhanced thermal conductivity of nanofluids. Journal of Nanoparticle Research, 5(1–2), 167–171.